DOI: 10.1002/chem.200901937

The Effect of Heavy Atoms on Photoinduced Electron Injection from Nonthermalized and Thermalized Donor States of M^{II}–Polypyridyl (M=Ru/Os) Complexes to Nanoparticulate TiO_2 Surfaces: An Ultrafast Time-Resolved Absorption Study

Sandeep Verma,[a] Prasenjit Kar,[b] Amitava Das,*[b] Dipak K. Palit,[a] and Hirendra N. Ghosh*[a]

Abstract: We have synthesized ruthenium(II)– and osmium(II)–polypyridyl complexes ($[M(bpy)_2\mathbf{L}]^{2+}$, in which $M=Os^{II}$ or Ru^{II}, bpy=2,2′-bipyridyl, and **L**=4-(2,2′-bipyridinyl-4-yl)benzene-1,2-diol) and studied the interfacial electron-transfer process on a TiO_2 nanoparticle surface using femtosecond transient-absorption spectroscopy. Ruthenium(II)- and osmium(II)-based dyes have a similar molecular structure; nevertheless, we have observed quite different interfacial electron-transfer dynamics (both forward and backward). In the case of the Ru^{II}/TiO_2 system, single-exponential electron injection takes place from photoexcited nonthermalized metal-to-ligand charge transfer (MLCT) states. However, in the case of the Os^{II}/TiO_2 system, electron injection takes place biexponentially from both nonthermalized and thermalized MLCT states (mainly ^{3}MLCT states). Larger spin–orbit coupling for the heavier transition-metal osmium, relative to that of ruthenium, accounts for the more efficient population of the ^{3}MLCT states in the Os^{II}-based dye during the electron-injection process that yields biexponential dynamics. Our results tend to suggest that appropriately designed Os^{II}–polypyridyl dye can be a better sensitizer molecule relative to its Ru^{II} analogue not only due to much broader absorption in the visible region of the solar-emission spectrum, but also on account of slower charge recombination.

Keywords: charge transfer · electron transfer · nanoparticles · photochemistry · spin–orbit coupling

Introduction

Sensitization of nanocrystalline TiO_2 electrodes with molecular chromophores forms the basis of efficient solar energy conversion in regenerative photoelectrochemical cells.[1] The study of interfacial electron-transfer dynamics involved in these solar cells is an area of intense interest as this provides the insight for understanding the dynamics of the photoinduced electron-injection process(es), which have been carried out in both experimental[1–14] and theoretical[15] investigations. These studies were expected to help in developing solar cells with better photon-to-current conversion efficiency (IPCE). In this context, Ru^{II}–[2–6,12] and Os^{II}–polypyridine complexes[7–11,13] have been used extensively by various researchers as the prospective photosensitizer molecule for the development of dye-sensitized solar cells (DSSCs).[2] The osmium complexes may have certain advantages when compared with the analogous ruthenium complexes, because the ruthenium polypyridyl-based photosensitizer molecules do not absorb solar photons below approximately 2.1 eV,[13] and as a result around 0.8 V is expected to be wasted in the reaction of $[Ru^{III}(bpy)_3]^{3+}$ (bpy=2,2′-bipyridyl) and I^- to sustain faradic current flow in the cell.[16] Os^{II}–polypyridyl complexes[2d,7–11,13,16–20], on account of their lower energy-absorption band in the visible region of the spectrum, may be more suitable for wider absorption of the solar spectrum

---

[a] S. Verma, Dr. D. K. Palit, Dr. H. N. Ghosh
Radiation and Photochemistry Division
Bhabha Atomic Research Centre, Mumbai 400 085 (India)
Fax: (+91) 22-25505151
E-mail: hnghosh@barc.gov.in

[b] P. Kar, Dr. A. Das
Central Salt and Marine Chemicals Research Institute
Bhavnagar 364002, Gujarat (India)
Fax: (+91) 278-567-562
E-mail: amitava@csmcri.org

Supporting information for this article, including details of ESMS spectra, transient spectra for the cation radicals, and additional figures, is available on the WWW under http://dx.doi.org/10.1002/chem.200901937.

and thus may act as a better sensitizer molecule in photoelectrochemical energy conversion.

In most of the studies reported so far—including very recent ones[2d]—the anchoring groups used to attach the metal–dye complexes to the nanoparticles are carboxylates.[1–11] However, use of carboxylates as an anchoring group has some disadvantages. The ground-state pK_a of the carboxylates is too low ($pK_a \approx 3.5$)[2b] to ensure strong binding, and in the presence of water, slow desorption of the photosensitizers may occur, which can limit the long-term stability of the cell. The pK_a value for the catecholate system is considerably higher ($pK_a > 9.6$), which ensures more efficient binding with TiO_2 nanoparticles, even at higher pH values.[5,12] It would therefore be interesting to synthesize catecholate-based osmium complexes and study the electron-transfer dynamics onto a TiO_2 nanoparticle surface.

In our earlier report,[13] we discussed the interfacial electron-transfer (IET) dynamics in a longer time domain (nanosecond) by monitoring charge-transfer emission involving Os^{II}-based sensitizer molecules bound to nanoparticulate TiO_2 through catecholate functionality using time-resolved emission spectroscopy. However, to understand the ET mechanism in this system in detail and the involvement of different MLCT states during the ET process, it is very important to study IET dynamics on an ultrafast timescale. It has been reported in the literature[3,4] that for related Ru^{II}–polypyridyl complexes the major component of the electron-transfer process(es) is extremely fast from the initially populated, vibronically nonthermalized excited singlet metal-to-ligand charge-transfer (^{1}MLCT) states prior to electronic and nuclear relaxation of the molecule. Simultaneous electron injection from the thermalized ^{3}MLCT states has also been observed and contributes to the multiexponential electron injection. In our earlier investigations[5,6] in which we used ruthenium–polypyridyl photosensitizers, namely, TiO_2 nanoparticles sensitized by $[Ru^{II}(bpy)_2(bp\text{-}CH{=}CH\text{-}catechol)]$[5] and $[Ru^{II}(SCN)_2(bpy)(bp\text{-}CH{=}CH\text{-}catechol)]$[6] (bpy = 2,2′-bipyridine), we observed only a single-exponential electron injection in TiO_2 CB (CB = conduction band) from photoexcited MLCT states. We also observed that the strong electronic coupling between dye–TiO_2 systems facilitates electron injection from nonthermalized MLCT states. The question that automatically arises is whether strong coupling should always facilitate single-exponential electron-injection kinetics or whether the energy of the photoexcited donor orbital(s) together with the rate of the intersystem-crossing (ISC) process influences the electron-transfer dynamics. To address this issue, we have synthesized ruthenium(II)– and osmium(II)–polypyridyl complexes ($[M(bpy)_2\mathbf{L}]^{2+}$ (in which M = Os^{II} or Ru^{II}, bpy = 2,2′-bipyridyl, and **L** = 4-(2,2′-bipyridinyl-4-yl)benzene-1,2-diol) and studied IET processes between nanoparticulate TiO_2 using femtosecond transient-absorption spectroscopy. In general, the ISC process is known to be much higher for the heavier metal ions like osmium due to higher spin–orbit coupling, so the choice of Os^{II} complex basically allows us to see the effect of lowering the energy of the excited singlet or triplet MLCT band of the donor orbital[6] and the ISC process on electron-injection dynamics.

Experimental Section

Materials: Titanium(IV) tetraisopropoxide ($Ti[OCH(CH_3)_2]_4$; Aldrich, 97 %), $RuCl_3{\cdot}x\,H_2O$, 2,2′-bipyridyl, 3,4-dimethoxybenzaldehyde, and acetaldehyde were procured from Sigma–Aldrich and were used as received. Pyridine and ethanol, used as solvent, were dried and distilled prior to use. Nanopure water (Barnsted System, USA) was used for making aqueous solutions. All other reagents were of analytical reagent grade and procured from S.D. Fine Chemicals (India). HPLC-grade acetonitrile (E. Mark, Bombay, India) was used for all spectrophotometric studies. Solvents were degassed thoroughly with Indian oxygen-limited analytical reagent (IOLAR)-grade dinitrogen gas before use in the preparation of all standard solutions. 3-(3,4-Dimethoxyphenyl)propanal (**A**), pyridacyl pyridinium iodide salt (**B**), and 4-(2,2′-bipyridinyl-4-yl)benzene-1,2-diol (**L**) were synthesized following previously reported procedures and are provided in the Supporting Information.

Analytical methods: Microanalyses (C, H, N) were performed using a Perkin–Elmer 4100 elemental analyzer. FTIR spectra were recorded either as KBr pellets or as solutions in acetonitrile in a cell fitted with a KBr window, using a Perkin–Elmer Spectra GX 2000 spectrometer. ^{1}H NMR spectra were recorded using a Bruker 200 MHz FT NMR spectrometer (model: Avance DPX 200) using CD_3CN as the solvent and tetramethylsilane (TMS) as an internal standard; ESIMS measurements were carried out using a Waters QTof-Micro instrument. Electronic spectra were recorded using a Shimadzu UV-3101 PC spectrophotometer; steady-state luminescence spectra were recorded using a Perkin–Elmer LS 50B luminescence spectrofluorimeter outfitted with a red-sensitive photomultiplier. Electrochemical experiments were performed using a CH-660A electrochemical instrument with a conventional three-electrode cell assembly. A saturated Ag/AgCl reference and a platinum working electrode were used for all measurements. Ferrocene was added at the end of each measurement of the cyclic voltammetric experiment as an internal standard and all potentials are quoted versus the ferrocene/ferrocenium (Fc/Fc^+) couple.

Nanoparticle preparation: Nanometer-sized TiO_2 was prepared by controlled hydrolysis of titanium(IV) tetraisopropoxide.[21–23] A solution of $Ti[OCH(CH_3)_2]_4$ (5 mL) dissolved in isopropyl alcohol (95 mL; Aldrich) was added dropwise ($1\,mL\,min^{-1}$) to nanopure water (900 mL; 2 °C) at pH 1.5 (adjusted with HNO_3). The solution was continuously stirred for 10–12 h until a transparent colloid was formed. The colloidal solution was concentrated at 35–40 °C with a rotary evaporator and then dried with a nitrogen stream to yield a white powder. In the present work all colloidal samples were prepared after dispersing the dry TiO_2 nanoparticles in water ($15\,g\,L^{-1}$).

Synthesis of complex 1: A solution of $[Ru(bpy)_2Cl_2]{\cdot}2\,H_2O$ (0.07 g, 0.072 mmol) and **L** (0.02 g, 0.07 mmol) dissolved in an ethanol/water mixture (1:1, v/v, 50 mL) was heated to reflux for 8 h with constant stirring under an inert atmosphere. Then ethanol was removed under vacuum and the desired crude complex was precipitated as a red-orange solid by adding an excess amount of aqueous KPF_6 solution. This was filtered off, washed with cold water, and air-dried. This crude product was further purified by gravity chromatography by using silica as the stationary phase and CH_3CN-saturated aqueous KPF_6 solution (98:2, v/v) as the eluent. Acetonitrile was then removed under vacuum, and the desired pure complex was extracted into the dichloromethane layer by solvent extraction. The dichloromethane was removed under reduced pressure to isolate the pure compound (0.070 g, 52 %). ^{1}H NMR (CD_3CN): $\delta = 8.70$ (d, $J = 9.0$ Hz, 2 H; $H^{6,6'}$ (**L**)), 8.51 (d, $J = 8.2$ Hz, 4 H; 2 $H^{6,6'}$ (bpy)), 8.06 (t, $J = 7.6$ Hz, 4 H; 2 $H^{4,4'}$ (bpy)), 7.82–7.58 (m, 7 H; 2 $H^{5,5'}$ (bpy), $H^{3,3',4'}$ (**L**)), 7.42–7.29 (m, 8 H; 2 $H^{3,3'}$ (bpy), 2 $H^{5,5'}$ (**L**), $H^{5,6}$ (phenyl)), 6.99 ppm (d, $J = 8.2$ Hz, 1 H; H^3 (phenyl)); IR (KBr): $\tilde{\nu} = 3450$ (-OH), 1604 (C=C, C=N), 842 cm^{-1} (PF_6); $E_{1/2}$ (vs. Ag/AgCl) $\{\Delta E\} = 1.32$ {102} ($Ru^{II/III}$), -1.38 {80}

(**L**/**L**$^{\cdot-}$), −1.62 {100} (bpy/bpy$^{\cdot-}$), −1.9 V {85 mV} (bpy/bpy$^{\cdot-}$); ESMS: *m*/*z* (%): 823 (29) [M^+-PF_6]; elemental analysis calcd (%) for **1**: C 44.68, H 2.92, N 8.69; found: C 44.7, H 2.8, N 8.5.

Synthesis of complex 2: A solution of [$Os(bpy)_2Cl_2$]·2 H_2O (0.070 g, 0.114 mmol) and **L** (0.030 g, 0.114 mmol) dissolved in an ethanol/water mixture (1:1, v/v, 50 mL) was heated to reflux for 16 h with constant stirring under an inert atmosphere. Ethanol was then removed under vacuum, and the desired crude complex was precipitated as a dark green solid by adding an excess amount of aqueous KPF_6 solution. This was filtered off, washed with cold water, and air-dried. This crude product was further purified by gravity chromatography by using silica as the stationary phase and CH_3CN-saturated aqueous KPF_6 solution (98:2, v/v) as the eluent. Acetonitrile was then removed under vacuum, and the desired pure complex was extracted into the dichloromethane layer by solvent extraction. The dichloromethane was removed under reduced pressure to isolate the pure compound (0.062 g, 52 %). ^{1}H NMR (CD_3CN): $\delta = 8.63$ (d, $J = 8.4$ Hz, 2 H; $H^{6,6'}$ (**L**)), 8.48 (d, $J = 8.2$ Hz, 4 H; 2 $H^{6,6'}$ (bpy)), 7.86 (t, $J = 7.8$ Hz, 4 H; 2 $H^{4,4'}$ (bpy)), 7.72–7.48 (m, 7 H; 2 $H^{5,5'}$ (bpy), $H^{3,3',4'}$ (**L**)), 7.37–7.27 (m, 8 H; 2 $H^{3,3'}$ (bpy), 2 $H^{5,5'}$ (**L**), $H^{5,6}$ (phenyl)), 6.99 ppm (d, $J = 8.2$ Hz, 1 H; H^3 (phenyl)); IR (KBr): $\tilde{\nu} = 3450$ (-OH), 1603 (C=C, C=N), 847 cm^{-1} (PF_6); $E_{1/2}$ (vs. Ag/AgCl) {ΔE} = 1.14 {105} ($Os^{II/III}$), −1.24 {80} (**L**/**L**$^{\cdot-}$),−1.48 {100} (bpy/bpy$^{\bullet-}$), −1.73 V {110 mV} (bpy/bpy$^{\bullet-}$); ESMS: *m*/*z* (%): 911 (85) [M^+-PF_6], 766 (60) [M^+-2PF_6]; elemental analysis calcd (%) for **2**: C 40.90, H 2.67, N 7.95; found: C 40.8, H 2.6, N 7.7.

Femtosecond visible spectrometer: The femtosecond tunable visible spectrometer was developed based on a multipass amplified femtosecond Ti:sapphire laser system from Avesta, Russia (1 kHz repetition rate at 800 nm, 50 fs, 800 μJ pulse^{-1}), and has been described earlier.[24,25] The 800 nm output pulse from the multipass amplifier is split into two parts to generate pump and probe pulses. In the present investigation, we have used both 800 nm (fundamental) and its frequency-doubled 400 nm as excitation sources. To generate pump pulses at 400 nm, one part of 800 nm with 200 μJ pulse^{-1} was frequency-doubled in β-BaB_2O_4 (BBO) crystals. To generate visible probe pulses, about 3 μJ of the 800 nm beam was focused onto a 1.5 mm-thick sapphire window. The intensity of the 800 nm beam was adjusted by iris size and neutral density filters to obtain a stable white light continuum in the 400 to over 1000 nm region. The probe pulses were split into the signal and reference beams and were detected by two matched photodiodes with variable gain. We kept the spot sizes of the pump beam and probe beam at the crossing point, which was around 500 and 300 μm, respectively. The excitation-energy density (at both 800 and 400 nm) was adjusted to approximately 2500 μJ cm^{-2}. The noise level of the white light was about 0.5 % with occasional spikes due to oscillator fluctuation. We have noticed that most laser noise is low-frequency noise and can be eliminated by comparing the adjacent probe laser pulses (pump blocked vs. unblocked using a mechanical chopper). The typical noise in the measured absorbance change is < 0.3 %. The instrument response function (IRF) for 400 nm excitation was obtained by fitting the rise time of the bleaching of the sodium salt of *meso*-tetrakis(4-sulfonatophenyl)porphyrin (TPPS) at 710 nm and was found to be 120 fs.

Results and Discussion

Synthesis of complexes 1 and 2: 3-(3,4-Dimethoxyphenyl)propanal (**A**) and pyridacyl pyridinium iodide salt (**B**$^+$I$^-$) were allowed to react for the synthesis of **Me$_2$L** by following the basic synthetic methodology generally adopted for the synthesis of pyridine derivatives (Scheme 1). Then the desired ligand **L** was obtained by reacting **Me$_2$L** with molten pyridinium hydrochloride salt at 190 °C. This ligand **L** was used for the reaction with [$Ru(bpy)_2Cl_2$] and [$Os(bpy)_2Cl_2$] for the synthesis of the desired complexes **1** and **2**, respectively. For the synthesis of complex **1**, [$Ru(bpy)_2Cl_2$]·2 H_2O was allowed to react at reflux temperature with one molar equivalent of **L** in ethanol as solvent, which was expected to yield the complex **1** in optimum yield. This was further purified by gravity chromatography. Analytical data matched well with the proposed formulation for this complex. Complex **2** was synthesized using the same procedure as adopted for complex **1**. Purity of the isolated complexes after column chromatography was checked by various analytical and spectroscopic methods. Analytical and spectroscopic data obtained for these two complexes agreed well with the proposed structure for the respective complexes.

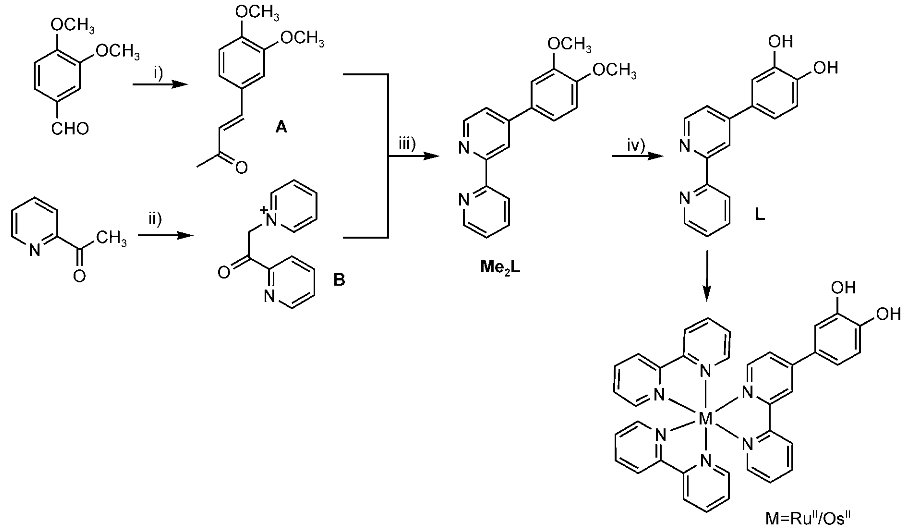

Scheme 1. Reaction scheme for the synthesis of 4-(2,2′-bipyridinyl-4-yl)benzene-1,2-diol (**L**) and complexes **1** and **2**. i) CH_3CHO, EtOH, 28 % NaOH, 0 °C, 30 min; ii) pyridine, I_2, reflux, 90 min, N_2 atmosphere; iii) CH_3COOH, $CH_3COO^-NH_4^+$; iv) pyridine–HCl, 190 °C, 180 min.

Cyclic voltammetry: Electrochemical studies revealed that $M^{II/III}$ redox potentials (with respect to the normal hydrogen electrode (NHE)) for complexes **1** and **2** are +1.32 ($Ru^{II/III}$) and +1.14 V ($Os^{II/III}$), respectively, and this difference in $M^{II/III}$ (M = Ru/Os) redox potential was reflected in the observed redshift of the MLCT band for the Os complex relative to the Ru complex.

UV/Vis absorption spectra: Prior to ultrafast transient absorption studies, we carried out steady-state absorption measurements of both the complexes in different media. Figure 1 shows the optical absorption spectra of complexes **1** and **2** and the respective complexes bound to nanoparticulate TiO_2 dispersed in water. Let us begin by discussing the optical absorption behavior of complex **1**. Figure 1a shows a low-energy band at 426 and 456 nm. The band at 426 nm can be attributed to a $d_{Ru^{II}}\rightarrow\pi^*_{bpy}$-based metal-to-ligand charge-transfer transition. The other band at 456 nm is attributed to $d_{Ru^{II}}\rightarrow\pi^*_{L}$-based MLCT transition. Since the excitation wavelength is 400 nm in the transient absorption measurements, we have not given much attention to characterizing the higher energy bands of Ru^{II} complexes. Now let us discuss the optical absorption behavior of complex **2**, which is shown in Figure 1b. Broad absorption bands with maxima at 443 and 486 nm (Figure 1b) are assigned to two $d_{Os^{II}}\rightarrow\pi^*_{bpy}$- (at ≈443 nm) and $d_{Os^{II}}\rightarrow\pi^*_{L}$-based (at ≈486 nm) MLCT transitions. The broad absorption feature exhibited by the Os^{II} complex (complex **2**) in the 550–750 nm region is attributed to spin-forbidden MLCT transitions, which gain intensity in the osmium complexes because of enhanced spin–orbit coupling, a common feature of heavy metal centers.[13,14] The absorption bands at 400–550 nm are attributed to the MLCT singlet state for complexes **1** and **2**.[5,13] After the addition of TiO_2 nanoparticles, the absorption spectrum (Figure 1c) of **1** becomes broad and redshifted with an appreciable increase in absorbance of the band at 460 nm. Once again, after the addition of TiO_2 nanoparticles, the absorption spectrum of complex **2** (Figure 1d) becomes broad and shifted to a longer wavelength with an appreciable increase in absorbance for both ($d\pi_{Os}\rightarrow\pi^*_{bpy}$ and $d\pi_{Os}\rightarrow\pi^*_{L}$) of the MLCT bands. Redshift and broadening of the visible band for both complexes **1** and **2** in the presence of TiO_2 could be attributed to the strong interaction between the sensitizer and nanoparticles.

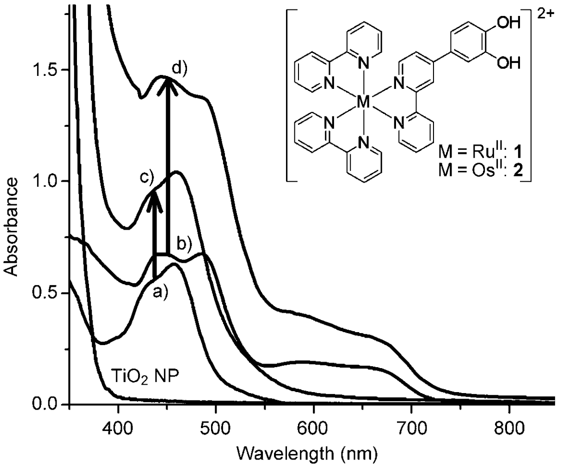

Figure 1. Optical absorption spectra of a) complex **1** in water, b) complex **2** in water, c) **1** on the TiO_2 nanoparticle surface, and d) **2** on the TiO_2 nanoparticle surface dispersed in water (the concentration of **1** was kept to around 38 μM, and that of **2** was kept to around 30 μM).

Excited-state dynamics of free complexes 1 and 2 in acetonitrile: To understand photoinduced interfacial electron-injection dynamics involving TiO_2 nanoparticles sensitized by complex **1** and **2**, it is essential to understand the excited-state dynamics of the sensitizer molecules in nonreactive media like acetonitrile. We have carried out femtosecond transient absorption studies in the visible and near-IR region to monitor the excited-state dynamics of the sensitizer molecules **1** and **2**. Figure 2 shows the transient absorption spectra of **1** at different time delays in acetonitrile following 400 nm laser-light excitation. The transients show a major absorption band in the 500–1000 nm wavelength region centered on 750 nm with simultaneous bleaching below the 500 nm region. The transient absorption bands can be ascribed to the excited-state absorption (ESA) of **1**. It has been reported in recent literature that an ISC process (singlet to triplet) for Ru^{II}–polypyridyl complexes is very fast (<50 fs).[26] Consequently, in the present investigation, we have attributed this ESA to the excited triplet-state (^{3}MLCT) absorption, as it is believed that the singlet-to-triplet conversion might have occurred within the pulse width of the instrument. It is interesting to observe that the ampli-

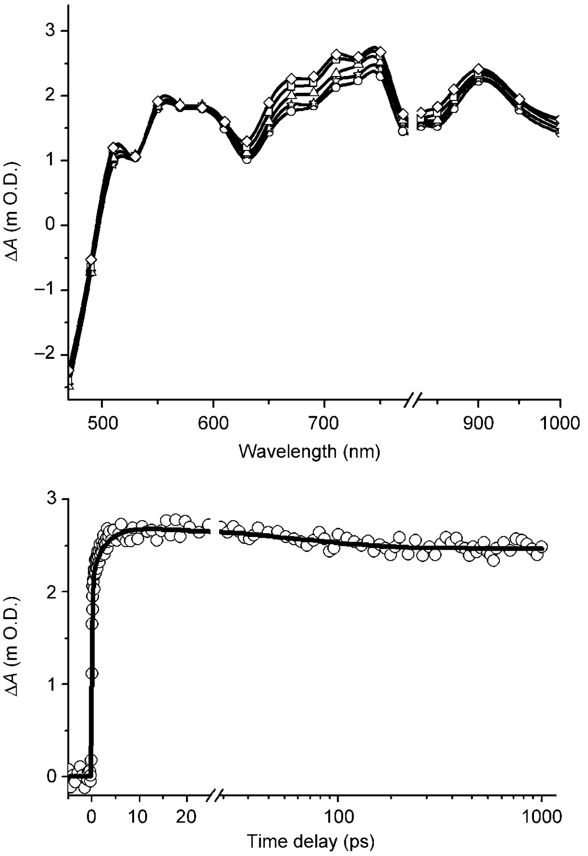

Figure 2. Transient absorption spectra of a solution of complex **1** in acetonitrile following excitation with a 400 nm laser pulse at 200 (○) and 500 fs (★) and 1 (△), 5 (□), and 10 ps (◇) time delays (top). Kinetic trace of the excited triplet state (^{3}MLCT) of **1** at 710 nm (bottom).

tude of the transient absorption increases with time (Figure 2), and after a certain time delay it does not decay for 1 ns. Figure 2 (bottom) shows the transient absorption decay kinetics at 710 nm for **1** in acetonitrile, and this could be best fit with time constants of <100 fs (94.3%) and 7 ps (6.7%). The first growth component is pulse-width limited (<100 fs), which can be attributed to the formation of the singlet and/or triplet MLCT state. However, the second component grows with a time constant of 7 ps and can be attributed to vibrational relaxation processes. As we can observe in Figure 1a, the absorption band of complex **1** extends up to 550 nm and on excitation at 400 nm it is quite natural that vibrationally hot (nonthermalized-state) molecules will be formed. This nonthermalized molecule will take some time to relax and reach the thermalized state, which can be attributed to vibrational relaxation. It is reported in the literature that the lifetimes of the triplet state (^{3}MLCT) of the analogous Ru^{II}–polypyridyl complexes are >100 ns or so.[27] Thus, the longer lifetime of the triplet state is actually reflected in the kinetic traces shown in Figure 2 (bottom), which does not decay for 1 ns.

Figure 3 shows the transient absorption spectra of a solution of complex **2** in acetonitrile following excitation with a 400 nm laser pulse with an approximately 100 fs pulse width. It shows bleaching in the 470–690 nm region and a broad positive absorption band in the 710–1000 nm region. The bleaching region consists of two peaks: one in the 470–490 nm region and another in the 530–690 nm region. Both the bleaching peak positions match well with absorbance peaks in the optical absorption spectra of complex **2** (see Figure 1b). Bleaching around the 470–510 nm region is due to the ^{1}MLCT absorption band and that in the 530–690 nm region is due to the spin-forbidden ^{3}MLCT absorption band. The spin–orbit coupling in the osmium complex is more prominent relative to that in the ruthenium complex. This allows a direct $^3\mathrm{MLCT}\leftarrow S_0$ transition, which results in extended optical absorption in the 530–690 nm region by the Os^{II}–polypyridyl complex. Therefore the bleaching in the 530–690 nm region can be attributed to the spin-forbidden $S_0\rightarrow{}^3\mathrm{MLCT}$ transition. The positive absorption band in the 710–1000 nm region is ascribed to mixed ^{1}MLCT and ^{3}MLCT excited-state absorption. It is well documented in the literature that the ISC process is very fast (<50 fs) in a heavy transition metal like osmium, so a pulse-width-limited ^{1}MLCT state to ^{3}MLCT state conversion is expected. Therefore, in the present investigation, the broad positive transient absorption band is dominated by the excited ^{3}MLCT state absorption. The transient decay profile monitored at 710 nm can be fit with biexponential time constants of $\tau_1=150$ ps (5.3%) and $\tau_2>1$ ns (94.75%). Long-lived species (>1 ns) can be attributed to MLCT triplet states of complex **2**.

Transient absorption measurements of 1/TiO$_2$ and 2/TiO$_2$: We have carried out transient absorption experiments for **1**/TiO$_2$ and **2**/TiO$_2$ systems following excitation with a laser source of 400 nm to explore the interfacial ET dynamics on the semiconductor surface. Figure 4 shows the transient absorption spectra of TiO$_2$ nanoparticles sensitized by complex **1** at different time delays. The spectrum at each time delay consists of bleaching below the 500 nm wavelength region, an absorption band at 510–630 nm that peaks at around 550 nm, and another broad positive absorption band in the 650–1000 nm region. The absorption peak at 550 nm can be attributed to **1**$^{\cdot+}$ (cation radical; see the Supporting Information). The broad absorption band in the 650–1000 nm region has been attributed to the conduction-band electrons in the nanoparticles.[22,28,29] Previously, it has been reported by us and many other research groups that conduction-band electrons can be detected by characteristic visible,[22,28,29] near-IR,[30] and mid-IR[3,31,32] absorption. Injection time in the present investigation was determined by monitoring the appearance time of the transient absorption signal of the injected electron ($e^-_{\mathrm{TiO_2}}$) at 1000 nm. Electron-injection dynamics (growth kinetics of the transient absorption signal) were found to be fit by a single exponential with a time constant of <100 fs. We discuss the mechanism of single-exponential electron-injection dynamics in the present system in detail in the next section. We have also monitored the

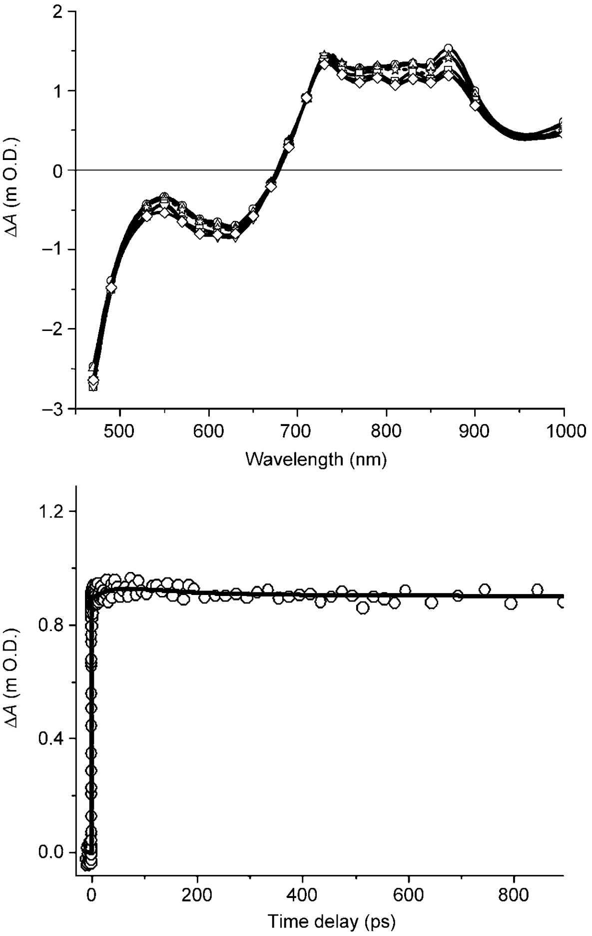

Figure 3. The transient absorption spectra of a solution of complex **2** in acetonitrile following excitation with a 400 nm laser pulse at 200 (○) and 500 fs (△) and 1 (★), 5 (□), 10 (▽), and 30 ps (◇) time delays (top). Kinetic trace of the excited triplet state (^{3}MLCT) of **2** at 710 nm (bottom).

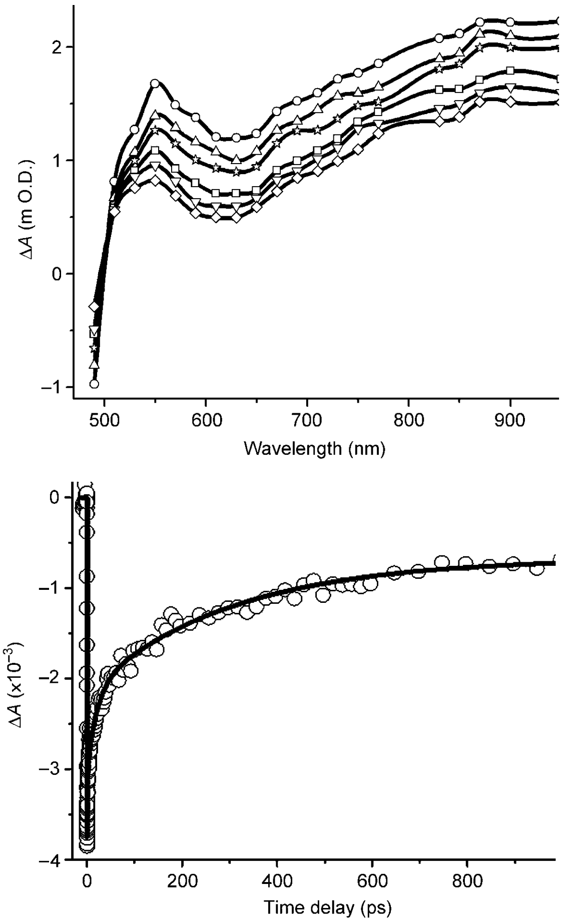

Figure 4. Transient absorption spectra of TiO_2 nanoparticles sensitized by **1** in water at 200 (○) and 500 fs (△) and 1 (★), 5 (□), 10 (▽), and 50 ps (◇) time delays after excitation at 400 nm (top). The kinetic trace at 490 nm (bottom).

bleaching at 490 nm, which primarily tells us the charge-recombination dynamics (back electron transfer, or BET) between the electron ($e^-_{TiO_2}$) and the parent cation (Ru^{III} center) to determine back-electron-transfer dynamics (shown in Figure 4, bottom). The bleaching recovery kinetics at 490 nm and transient decay kinetics at 1000 nm for the **1**/TiO_2 system can be fit with multiexponential time constants of $\tau_1 = 0.8$ ps (29 %), $\tau_2 = 20$ ps (21 %), and $\tau_3 > 300$ ps (50 %).

We have also carried out transient absorption studies with the **2**/TiO_2 system following excitation with a laser light at 400 nm. Figure 5 shows the transient absorption spectra of TiO_2 nanoparticles sensitized by **2** at different time delays. Here the absorption band at 550 nm has also been attributed to the cation radical ($\mathbf{2}^{\cdot +}$; see the Supporting Information) and the broad band in the wavelength region 700–1000 nm can be attributed to the injected electron in the conduction band in TiO_2 nanoparticles ($e^-_{TiO_2}$). We have assigned the cation radical of **2** on the basis of the results obtained in a complementary pulse radiolysis experiment, in which $\mathbf{2}^{\cdot +}$ was generated selectively by the reaction of the N_3 radical with **2** in N_2O saturated aqueous solution (5 % acetonitrile+95 % water) and is shown in the Supporting Information. Transient absorption spectra show two negative absorption bands peaking at 490 and 600 nm; these can be attributed to the bleaching due to ground-state absorption (Figure 1d). The injection time in the present investigation was determined by monitoring the appearance signal of the injected electron ($e^-_{TiO_2}$) at 1000 nm. The electron-injection dynamics (growth kinetics in the transient absorption signal) in the **2**/TiO_2 system can be fit with biexponential time constants of $\tau^1_{inj} < 100$ fs (42 %) and $\tau^2_{inj} = 1.7$ ps (58 %). The mechanism of biexponential electron injection in strongly coupled dye–nanoparticle systems is discussed in the next section. We have also monitored the bleaching at 490 nm, which primarily gives the time constants of the BET between the injected electron and the parent cation (Os^{III}). The bleaching recovery kinetics at 490 nm (Figure 5, bottom) and transient decay kinetics at 1000 nm (Figure 6B) for the **2**/TiO_2 system can be fit with multiexponential time constants of $\tau_1 = 2.0$ ps (12 %), $\tau_2 = 35$ ps (17 %), and $\tau_3 >$ 300 ps (71 %).

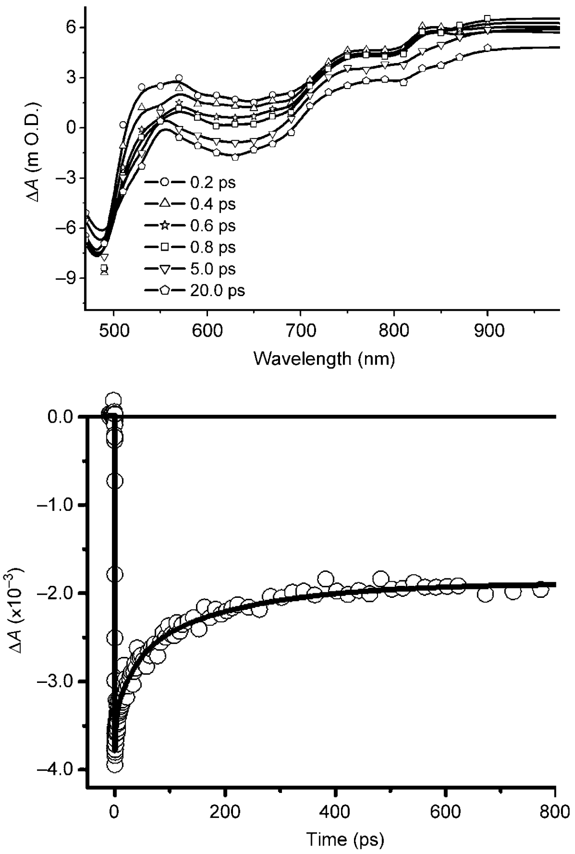

Figure 5. Transient absorption spectra of TiO_2 nanoparticles sensitized by **2** in water at 200, 400, 600, and 800 fs and 5 and 20 ps time delays after excitation at 400 nm. Bottom: The kinetic trace at 490 nm.

Interfacial electron-transfer dynamics: Interfacial electron-transfer dynamics in ruthenium–polypyridyl complexes—in particular [Ru(dcbpy)$_2$(NCS)$_2$], widely known as the ruthenium–N3 complex (dcbpy = 4,4′-(dicarboxylic acid)-2,2′-bi-

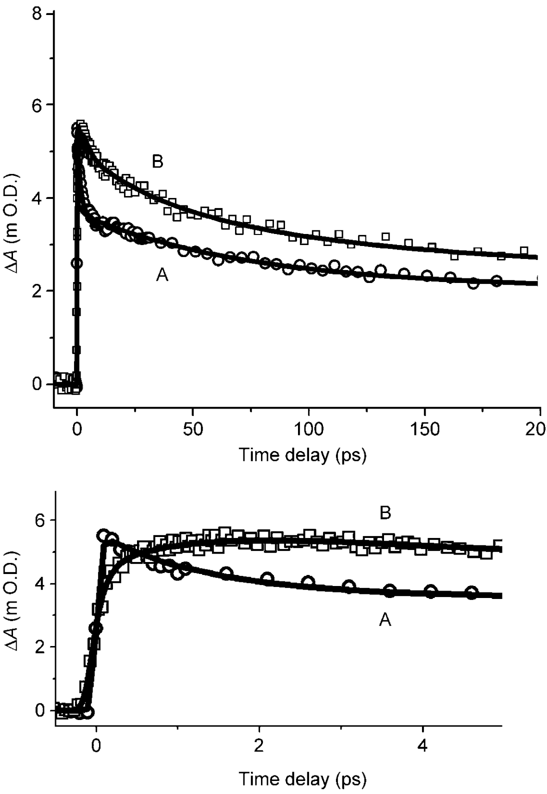

Figure 6. Kinetic decay trace of the injected electron in the conduction band at 1000 nm in **1**/TiO_2 (A) and **2**/TiO_2 (B) following excitation with a 400 nm laser pulse. Bottom: The kinetic trace on a shorter timescale.

pyridine)-sensitized TiO_2 nanomaterials—has been a subject of intense research interest for more than a decade. It has been shown by femtosecond transient IR and near-IR spectroscopy that in most of the cases[3] injection happens in the ultrafast time domain and occurs prior to vibrational relaxation of the thermally equilibrated MLCT manifold (i.e., from "hot" excited states or the Frank–Condon state itself). However, most authors have argued in favor of the presence of a sub-100 fs component and considered it to be the dominant channel with additional contributions of slower nonexponential electron injection with a distribution of characteristic times from 1 ps to tens of picoseconds. Durrant et al.[33] reported biexponential electron injection (EI) with <150 fs (50%) and approximately 1.2 ps (50%) time constants for a carboxylate-functionalized $[Ru^{II}(dcbpy)_2(NCS)_2]/TiO_2$ system, in which the slower component was attributed to thermalized MLCT states. It has been clearly demonstrated by Benko et al.[4] that electron injection in the Ru–N3/TiO_2 system occurs mainly from the nonthermalized ^{1}MLCT state with a smaller contribution from the ^{3}MLCT state. Later, Piotrowiak and co-workers[34] reported multiexponential electron-injection kinetics in a $[Ru(bpy)_2(dcbpy)]/TiO_2$ system. Lewis and McCusker[10] also reported multiexponential EI in structurally identical Ru^{II}– and Os^{II}–polypyridyl complexes with carboxylate anchoring on the TiO_2 surface. Interestingly, in all such cases multiexponential electron-injection dynamics were observed for carboxylate sensitizers in which electronic coupling is considered to be moderate with TiO_2 nanoparticulate. However, in our earlier investigation,[5,6] we reported only a single exponential and pulse-width-limited (<100 fs) electron injection from photoexcited MLCT states into the conduction band of TiO_2 nanoparticles. In those we used $[Ru(bpy)_2(bp\text{-}CH{=}CH\text{-}catechol)]$[5] and $[Ru(bpy)(SCN)_2(bp\text{-}CH{=}CH\text{-}catechol)]$[6] as the photosensitiser, in which the sensitizers are coupled strongly with the nanoparticles through catecholate binding. Therein we have demonstrated that the electron-injection process competes with the thermalization process in the photoexcited state of strong coupling dye molecules. Our earlier results indicated that electron injection took place predominantly from the nonthermalized singlet state (^{1}MLCT) and/or the nonthermalized triplet state (^{3}MLCT) or a combination of both. Strong coupling in dye–nanoparticle systems facilitates ultrafast single-exponential electron injection, which competes with the thermalization process of the excited states.

To find out whether strong coupling always gives single-exponential injection and how the presence of heavy atoms affects electron injection in strongly coupled dye–nanoparticle systems, we have carried out transient absorption studies in structurally similar ruthenium– and osmium–polypyridyl complexes with a catechol moiety on the TiO_2 nanoparticle surface. In an earlier section, we discussed transient absorption measurements in both **1**/TiO_2 and **2**/TiO_2 systems. To compare the electron-transfer dynamics (both electron injection and BET), the transient absorption signals at 1000 nm following excitation with 400 nm laser pulses for complexes **1** and **2** on the TiO_2 nanoparticle surface are shown in Figure 6. Traces on a shorter timescale are shown as in Figure 6, bottom. It is evident from curve A (shown in the bottom of Figure 6) that the electron-injection kinetics in **1**/TiO_2 are single exponential with a pulse-width-limited ($<$ 100 fs) time constant. This single-exponential electron injection for **1**/TiO_2 could be attributed to the injection from nonthermalized MLCT states. Here, due to strong coupling through the catecholate moiety, electron injection competes with the ISC rate, which leads to thermalized ^{3}MLCT states. On the other hand, in the **2**/TiO_2 system (shown in curve B), electron-injection dynamics are found to be biexponential with time constants of $\tau^1_{inj} < 100$ fs (42%) and $\tau^2_{inj} = 1.7$ ps (58%). Here the shorter component could be attributed to the electron injection from nonthermalized MLCT states and the longer component could be attributed to electron injection predominantly from thermalized ^{3}MLCT states. In Scheme 2, we have shown the mechanistic pathways of electron transfer and the relaxation dynamics of both dyes (**1** and **2**) bound to the TiO_2 surface. The ground- and excited-state energy levels of these complexes were determined by cyclic voltammetry and the optical absorption spectrum of MLCT-based singlet and triplet states. It is interesting to see that the ET pathways are different for the two complexes, even though the energy levels of the complexes do not differ appreciably. As Os is the heavier transition metal, the spin–orbit coupling for Os^{II} complexes is larger relative to analogous Ru^{II} complexes and for complex **2** the ISC pro-

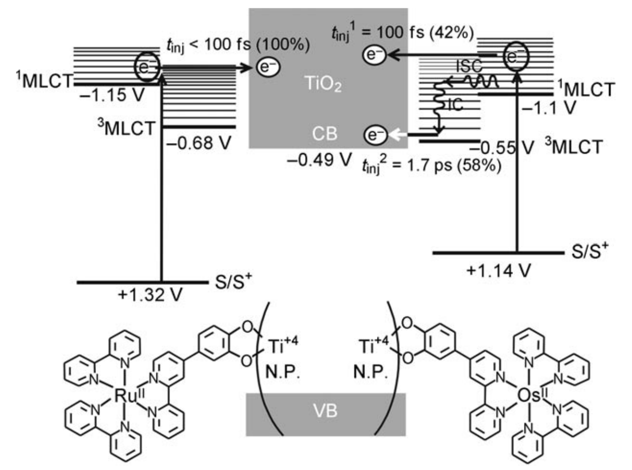

Scheme 2. Mechanistic scheme showing a three-level model that consists of the ground state (S_0), excited triplet state (^{3}MLCT), and excited singlet (^{1}MLCT) state of **1** and **2** adsorbed on TiO_2 nanoparticles. CB = Conduction band; VB = valence band.

cess is therefore expected to be much faster and more efficient. Thus upon photoexcitation the ^{3}MLCT state gets populated much faster through an efficient ISC process from initially populated ^{1}MLCT states relative to the analogous Ru^{II} complex **1** and electron injection takes place from both the states with different time constants (Scheme 2).

We have also monitored back-electron-transfer (BET) time constants for both the systems by monitoring kinetic decay traces at 1000 nm as well as bleaching recovery kinetics at 490 nm for both the systems. BET kinetics for the **1**/TiO_2 system can be fit with multiexponential time constants of $\tau_1 = 0.8$ ps (29 %), $\tau_2 = 20$ ps (21 %), and $\tau_3 > 300$ ps (50 %), and for the **2**/TiO_2 system the kinetics can be best fit with time constants of $\tau_1 = 2.0$ ps (12 %), $\tau_2 = 35$ ps (17 %), and $\tau_3 > 300$ ps (71 %). Interestingly, the BET dynamics have been found to be slower in the **2**/TiO_2 system relative to the **1**/TiO_2 system. Furthermore, we have also confirmed that in a longer time domain (up to 500 μs) the BET reaction is slower in the **2**/TiO_2 system relative to the **1**/TiO_2 system (see the Supporting Information).

Conclusion

We have synthesized a ruthenium(II)– and an osmium(II)–polypyridyl complex ($[M(bpy)_2\mathbf{L}]^{2+}$, in which M = Ru^{II} (**1**) or Os^{II} (**2**), bpy = 2,2′-bipyridyl, and **L** = 4-(2,2′-bipyridinyl-4-yl)benzene-1,2-diol), and characterized them by means of various analytical and spectroscopic techniques. Optical absorption studies show that complex **1** has a strong MLCT absorption band at 400–500 nm, which is attributed to a ^{1}MLCT (spin-allowed) transition. Complex **2**, however, featured two strong MLCT absorption bands in the 400–550 and 550–750 nm regions, which are attributed to ^{1}MLCT (spin-allowed) and ^{3}MLCT (spin-forbidden) transitions. The pendant catecholate moiety of the complexes allows complexes **1** and **2** to couple strongly with the nanoparticles with the formation of a charge-transfer complex. Femtosecond transient absorption measurements have been carried out to study IET dynamics in both [Ru^{II}(bpy)$_2$(bp-catehol)]/TiO_2 (namely, **1**/TiO_2) and [Os^{II}(bpy)$_2$(bp-catehol)]/TiO_2 (namely, **2**/TiO_2) systems. Upon excitation with a 400 nm laser pulse, bleaching of the adsorbed dye, transient absorption for the dye cations ($M^{\cdot+}$), and a broad absorption band for the conduction-band electron are observed. Electron injection is found to be single exponential and pulse-width limited (< 100 fs) in the **1**/TiO_2 system, thereby indicating injection from the nonthermalized singlet state (^{1}MLCT), and/or nonthermalized triplet state (^{3}MLCT), or a combination of both. On the other hand, in the **2**/TiO_2 system electron-injection dynamics are found to be biexponential with time constants of $\tau_{inj}^1 < 100$ fs (42 %) and $\tau_{inj}^2 = 1.7$ ps (58 %). Here the shorter component could be attributed to the electron injection from nonthermalized MLCT states and the longer component could be attributed to electron injection from thermalized ^{3}MLCT states. Back-electron-transfer (BET) dynamics were studied by monitoring the decay kinetics of the cation radical, the injected electron in the conduction band of TiO_2, and also from recovery kinetics of the bleaching of the adsorbed dye. BET kinetics for the **1**/TiO_2 system can be fit with multiexponential time constants of $\tau_1 = 0.8$ ps (29 %), $\tau_2 = 20$ ps (21 %), and $\tau_3 > 300$ ps (50 %), and for the **2**/TiO_2 system the kinetics can be best fit with time constants of $\tau_1 = 2.0$ ps (12 %), $\tau_2 = 35$ ps (17 %), and $\tau_3 > 300$ ps (71 %). It is interesting to see that BET dynamics are slower for the **2**/TiO_2 system than the **1**/TiO_2 system.

Acknowledgements

We thank Dr. T. Mukherjee and Dr. S. K. Sarkar of BARC, and Dr. P. K. Ghosh of CSMCRI for their constant encouragement. H.N.G. thanks BRNS, and A.D. thanks DST and BRNS for financial assistance.

[1] B. O'Regan, M. Grätzel, *Nature* **1991**, *353*, 737.

[2] a) S. Ardo, G. J. Meyer, *Chem. Soc. Rev.* **2009**, *38*, 115; b) M. K. Nazeeruddin, P. Pechy, T. Renouard, S. M. Zakeeruddin, R. Humphry-Baker, P. Comte, P. Liska, L. Cevey, E. Costa, V. Shklover, L. Spiccia, G. B. Deacon, C. A. Bignozzi, M. Gratzel, *J. Am. Chem. Soc.* **2001**, *123*, 1613; c) M. K. Nazeeruddin, S. M. Zakeeruddin, R. Humphry-Baker, M. Jirousek, P. Liska, N. Vlachopoulus, V. Skhlover, C. H. Fischer, M. Gratzel, *Inorg. Chem.* **1999**, *38*, 6298; d) D. Kuciauskas, M. S. Freund, H. B. Gray, J. R. Winkler, N. S. Lewis, *J. Phys. Chem. B* **2001**, *105*, 392; e) S. Altobello, R. Argazzi, S. Caramori, C. Contado, S. Da Fre, P. Rubino, C. Choné, G. Larramona, C. A. Bignozzi, *J. Am. Chem. Soc.* **2005**, *127*, 15342; f) F. Gao, Y. Wang, J. Zhang, D. Shi, M. Wang, R. Humphry-Baker, P. Wang, S. M. Zakeeruddin, M. Grätzel, *Chem. Commun.* **2008**, 2635; g) B. Dietzek, W. Kiefer, J. Blumhoff, L. Bçttcher, S. Rau, D. Walther, U. Uhlemann, M. Schmitt, J. Popp, *Chem. Eur. J.* **2006**, *12*, 5105.

[3] J. B. Asbury, E. Hao, Q. Y. Wang, H. N. Ghosh, T. Lian, *J. Phys. Chem. B* **2001**, *105*, 4545.

[4] G. Benkö, J. Kallioinen, J. E. I. Korppi-Tommola, A. P. Yartsev, V. Sundstrom, *J. Am. Chem. Soc.* **2002**, *124*, 489.

[5] G. Ramakrishna, D. A. Jose, D. KrishnaKumar, A. Das D. K. Palit, H. N. Ghosh, *J. Phys. Chem. B* **2005**, *109*, 15445.

[6] P. Kar, S. Verma, A. Das, H. N. Ghosh, *J. Phys. Chem. C* **2009**, *113*, 7970.
[7] G. Sauvé, M. E. Cass, S. J. Doig, I. Lauermann, K. Pomykal, N. S. Lewis, *J. Phys. Chem. B* **2000**, *104*, 3488.
[8] C. Chiorboli, M. A. J. Rodgers, F. Scandola, *J. Am. Chem. Soc.* **2003**, *125*, 483.
[9] T. A. Heimer, E. J. Heilweil, C. A. Bignozzi, G. J. Meyer, *J. Phys. Chem. A* **2000**, *104*, 4256.
[10] D. Kuciauskas, J. E. Monat, R. Villahermosa, H. B. Gray, N. S. Lewis, J. K. McCusker, *J. Phys. Chem. B* **2002**, *106*, 9347.
[11] P. G. Hoertz, D. W. Thompson, L. A. Friedman, G. J. Meyer, *J. Am. Chem. Soc.* **2002**, *124*, 9690.
[12] C. R. Rice, M. D. Ward, M. K. Nazeeruddin, M. Gratzel, *New J. Chem.* **2000**, *24*, 651.
[13] S. Verma, P. Kar, A. Das, D. K. Palit, H. N. Ghosh, *J. Phys. Chem. C* **2008**, *112*, 2918.
[14] E. M. Kober, J. V. Caspar, B. P. Sullivan, T. J Meyer, *Inorg. Chem.* **1988**, *27*, 4587.
[15] a) L. G. C. Rego, V. S. Batista, *J. Am. Chem. Soc.* **2003**, *125*, 7989; b) W. R. Duncan, O. V. Prezhdo, *Annu. Rev. Phys. Chem.* **2007**, *58*, 143, and references therein. c) A. Petersson, M. Ratner, H. O. Karlsson, *J. Phys. Chem. B* **2000**, *104*, 8498; d) D. A. Gaal, J. E. McGarrah, F. Liu, J. E. Cook, J. T. Hupp, *Phys. Chem. Chem. Phys.* **2007**, *9*, 853.
[16] A. Hagfeldt, M. Gratzel, *Chem. Rev.* **1995**, *95*, 49.
[17] D. Xu, J. Z. Zhang, B. Hong, *J. Phys. Chem. A* **2001**, *105*, 7979.
[18] H. B. Baudin, J. Davidsson, S. Serroni, A. Juris, V. Balzani, S. Campagna, L. Hammarstrom, *J. Phys. Chem. A* **2002**, *106*, 4312.
[19] F. Barigelletti, L. De Cola, V. Balzani, R. Hage, J. G. Haasnoot, J. Reedijk, J. G. Vos, *Inorg. Chem.* **1991**, *30*, 641.
[20] R. Argazzi, G. Larramona, C. Contado, C. A. Bignozzi, *J. Photochem. Photobiol. A* **2004**, *164*, 15.
[21] D. Bahnemann, A. Henglein, J. Lilie, L. Spanhel, *J. Phys. Chem.* **1984**, *88*, 709.
[22] H. N. Ghosh, *J. Phys. Chem. B* **1999**, *103*, 10382.
[23] G. Ramakrishna, H. N. Ghosh, *Langmuir* **2003**, *19*, 505.
[24] D. Kuciauskas, M. S. Freund, H. B. Gray, J. R. Winkler, N. S. Lewis, *J. Phys. Chem. B* **2001**, *105*, 392.
[25] S. Kaniyankandy, S. Verma, J. A. Mondal, D. K. Palit, H. N. Ghosh, *J. Phys. Chem. C* **2009**, *113*, 3593.
[26] A. C. Bhasikuttan, M. Suzuki, S. Nakashima, T. Okada, *J. Am. Chem. Soc.* **2002**, *124*, 8398.
[27] A. Vlèek, Jr., *Coord. Chem. Rev.* **2000**, *200*, 933.
[28] J. Z Zhang, *Acc. Chem. Res.* **1997**, *30*, 423.
[29] D. P. Colombo, Jr., R. M. Bowman, *J. Phys. Chem.* **1996**, *100*, 18445.
[30] T. Hannappel, B. Burfeindt, W. Storck, F. Willig, *J. Phys. Chem. B* **1997**, *101*, 6799.
[31] H. N. Ghosh, J. B. Asbury, T. Lian, *J. Phys. Chem. B* **1998**, *102*, 6482.
[32] J. B. Asbury, R. J. Ellingson, H. N. Ghosh, S. Ferrere, A. Nozik, T. Lian, *J. Phys. Chem. B* **1999**, *103*, 3110.
[33] Y. Tachibana, J. E. Moser, M. Grätzel, D. R. Klug, J R. Durrant, *J. Phys. Chem.* **1996**, *100*, 20056.
[34] T. D. M. Bell, C. Pagba, M. Myahkostupov, J. Hofkens, P. Piotrowiak, *J. Phys. Chem. B* **2006**, *110*, 25314.

Received: July 13, 2009